PHYSICAL REVIEW A **83**, 053633 (2011)

Magnetic merging of ultracold atomic gases of ^{85}Rb and ^{87}Rb

S. Händel, T. P. Wiles, A. L. Marchant, S. A. Hopkins, C. S. Adams, and S. L. Cornish
Department of Physics, Durham University, Durham DH1 3LE, United Kingdom

(Received 3 March 2011; published 27 May 2011)

We report the magnetic merging of ultracold atomic gases of ^{85}Rb and ^{87}Rb by the controlled overlap of two initially spatially separated magnetic traps. We present a detailed analysis of the combined magnetic-field potential as the two traps are brought together that predicts a clear optimum trajectory for the merging. We verify this prediction experimentally using ^{85}Rb and find that the final atom number in the merged trap is maximized with minimal heating by following the predicted optimum trajectory. Using the magnetic-merging approach allows us to create variable-ratio isotopic Rb mixtures with a single laser-cooling setup by simply storing one isotope in a magnetic trap before jumping the laser frequencies to the transitions necessary to laser cool the second isotope.

DOI: 10.1103/PhysRevA.83.053633 PACS number(s): 03.75.−b

I. INTRODUCTION

The production of mixtures of two or more ultracold atomic gases [1–12] provides access to a diverse range of exciting phenomena [13–18]. Many of these phenomena result from the fact that the component species in the mixture can have notably different intrinsic properties, such as different spins, masses, collision cross sections, optical polarizabilities, and quantum statistics. Atomic mixtures have also come to prominence in the production of ultracold heteronuclear molecules [19] through magnetoassociation [20,21] and/or optical association [22]. Indeed, the recent production of ultracold molecules in the rovibrational ground state [23–28] from ultracold atomic gases brings the realm of dipolar molecular quantum gases [29] within reach. In addition to possessing the above intrinsic interest, mixtures play an important technical role in the sympathetic cooling of difficult bosonic species such as ^{85}Rb [10,30] and ^{41}K [31] and all fermions [32] owing to the suppression of s-wave scattering for fermions. However, the realization of some mixtures can be challenging due to detrimental light-assisted inelastic collisions between the two species [33,34].

A mixture of ^{85}Rb and ^{87}Rb has several attractive features for quantum gas studies. There exist two interspecies Feshbach resonances [35] suitable for the production heteronuclear molecules [36]. The interspecies elastic cross section is favorable for sympathetic cooling of ^{85}Rb [35], initially demonstrated in Ref. [37] and later used to reach quantum degeneracy by two groups [10,30]. The broad intraspecies Feshbach resonance in ^{85}Rb has been extensively used to control the atomic interactions in a Bose-Einstein condensate [38], permitting the study of the collapse of a condensate [39,40] and the formation of bright matter-wave solitons [41], as well as enabling the investigation of phase separation in a dual-species ^{85}Rb-^{87}Rb condensate [10].

In this paper we report a scheme to prepare ultracold mixtures using two magnetic traps that are controllably merged to combine the two atomic gases. The scheme has general applicability in that any pair of magnetically trappable species could be merged. However, the merging of two initially separated trapping potentials is nontrivial and the bulk of this paper is devoted to a detailed theoretical and experimental study of this process. In particular, we provide a detailed analysis of the combined magnetic-field potential during the merging process that highlights the optimum merging trajectory. This analysis significantly extends the previous experimental study [42] and should have general applicability for any similar trap-merging experiments. We convincingly demonstrate the validity of our analysis with a specific example, the merging of ultracold atomic gases of ^{85}Rb and ^{87}Rb.

The overall sequence of our experiment is as follows. Ultracold atoms are collected from a background vapor in a magneto-optical trap (MOT), loaded into a magnetic quadrupole trap (trap 1) and transported [43,44] from the MOT chamber to an UHV glass cell using a motorized translation stage [Fig. 1(a)]. The atoms are then transferred into a static quadrupole trap (trap 2) and trap 1 is moved back to the MOT chamber. At the same time the laser frequencies are jumped to the transitions necessary to laser cool the second isotope. A second sample of atoms is collected and again transported to the UHV cell where the two traps are controllably merged. Hence we are able to realize the production of a mixture of the two Rb isotopes by magnetic merging with only a single-laser-cooling setup.

The structure of the paper is as follows. In Sec. II we describe the calculations of the magnetic potential that lead to the prediction of an optimum merging trajectory. We present our experimental apparatus in Sec. III. In Sec. IV we describe experiments that test the predictions of our magnetic potential analysis and verify that the predicted optimum trajectory maximizes the final atom number in the merged trap with minimal heating of the gas. Finally, we demonstrate merging of variable proportions of the two different isotopes of rubidium.

II. THEORY

The magnetic traps employed in the experiment are simple quadrupole traps generated using two circular coils in which the currents flow in opposite directions. The resulting magnetic field increases linearly in all directions from a field zero located on axis midway between the coils. The traps are characterized by their axial field gradient, which is twice the radial gradient. Due to adiabatic following, the magnetic potential U_{mag} experienced by an atom is proportional to the

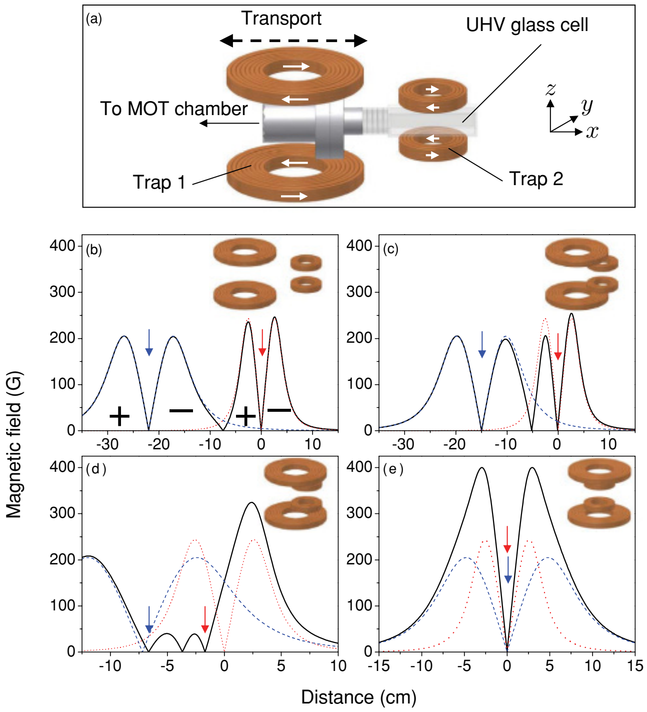

FIG. 1. (Color online) (a) Schematic of the experiment. A cloud of ultracold atoms is transported from the MOT chamber in a quadrupole trap (trap 1) mounted on a motorized translation stage. Trap 1 reaches the UHV glass cell and the cloud is transferred into the static quadrupole trap (trap 2). Trap 1 then returns to the MOT chamber, collects a second cloud, and is merged with the static trap. (b)–(e) The magnitude of the magnetic field along the x axis for trap 1 (dashed blue curve), trap 2 (dotted red curve), and the sum (solid black curve) for different separations of the coils. (b) Separation 22.5 cm: There are two separate quadrupole traps. The + and − signs indicate the direction of the field. (c) Separation 15 cm: As trap 1 approaches trap 2 an additional quadrupolelike zero is created where the dotted red and the dashed blue curves cross and the opposing signs of the field cause cancellation. The two inner barriers in the magnetic potential prevent the atoms from entering the central trap. (d) Separation 7.5 cm: The height of the inner barriers is significantly reduced as the separation of the traps is decreased. However, the atoms are still confined in the two outer traps. Note that the gradient ratio has been adjusted between (c) and (d) to maintain two inner barriers of the same height. (e) Separation 0 cm: Once merging is complete, both traps are overlapped to create a single quadrupole trap.

magnitude of the field, i.e., $U_{\text{mag}} = m_F g_F \mu_B |B|$ [45], where m_F is the magnetic sublevel, g_F is the Landé g factor, and μ_B is the Bohr magneton. However, as the two traps merge the magnetic fields add vectorially so that the local direction of the magnetic field is also important. The potential that results from the interference of the two magnetic fields as the traps merge depends sensitively on the field generated by each coil. Consequently, to understand the merging process we calculate the combined magnetic potential resulting from both quadrupole traps as the distance between them is varied.

The magnetic field generated by each coil is calculated by numerical integration of the Biot-Savart law

$$\mathbf{B} = \int \frac{\mu_0 I'}{4\pi} \frac{d\mathbf{l} \times \mathbf{r}}{|\mathbf{r}|^3}, \tag{1}$$

where μ_0 is the permeability of free space, I' is the current through the coil, $d\mathbf{l}$ is an infinitesimally small element of the coil, and $\mathbf{r}$ is the vector from the element $d\mathbf{l}$ to the point in space where the magnetic field is to be calculated. The total magnetic field is then found by summing the contributions from each coil. In the experiment the real coils are wound from multiple turns of square cross-section copper tubing with the dimensions summarized in the Appendix. For simplicity, the coils are approximated by equivalent coils consisting of a single turn of infinitesimal thickness and carrying a current of $I' = NI$, where N is the number of turns of the real coil and I is the current in the real coil. The radii and separations of the equivalent coils were found by matching the calculated first and third spatial derivatives to the measured values for the real coils. Comparing the measured and calculated magnetic fields results in a normalized rms deviation of approximately 1% over the range of interest, confirming the validity of this approximation.

We performed the calculation of the combined magnetic potential on a three-dimensional grid spanning both traps. From this grid we generated one-dimensional cuts, two-dimensional contours, and three-dimensional isosurfaces of this potential. A preliminary analysis revealed that the essential details of the merging process could be extracted from the simpler one-dimensional cuts of the combined magnetic potential along the line joining the two trap centers. Examples of such one-dimensional cuts are shown in Figs. 1(b)–1(e), where the magnetic field due to traps 1 and 2 and the combined magnetic field are indicated by the dashed blue, dotted red, and solid black lines, respectively. For a given set of coils the form of the combined magnetic potential depends critically on two parameters: the separation of the two trap centers and the ratio of the axial magnetic-field gradients at each trap center (trap 2:trap 1), henceforth referred to as the gradient ratio. Our insight is that successful merging requires that we follow the idealized merging scenario shown in Figs. 1(b)–1(e) in which the inner barriers of the magnetic potential that separate the two traps are maintained at equal heights throughout the merging. We stress that this is not usually the case when two magnetic quadrupole traps are simply moved toward each other and requires that the gradient ratio (and therefore the currents in each coil) be adjusted as the trap centers approach each other.

To fully explore the merging process a set of approximately 1000 one-dimensional plots of combined magnetic potential was generated for varying trap separations and gradient ratios. To condense this grid of plots into a more useful form we identified regions where qualitatively similar behavior was present in the combined magnetic potential, such as the presence of three field zeros or the existence of a single merged trap. These regions are shown in Fig. 2(a) as a function of trap center separation and gradient ratio. Each merging event has a unique trajectory through this potential map, traveling from left to right on the figure. Examples of four individual points in Fig. 2(a) are shown in Figs. 2(b)–2(e) in order to demonstrate

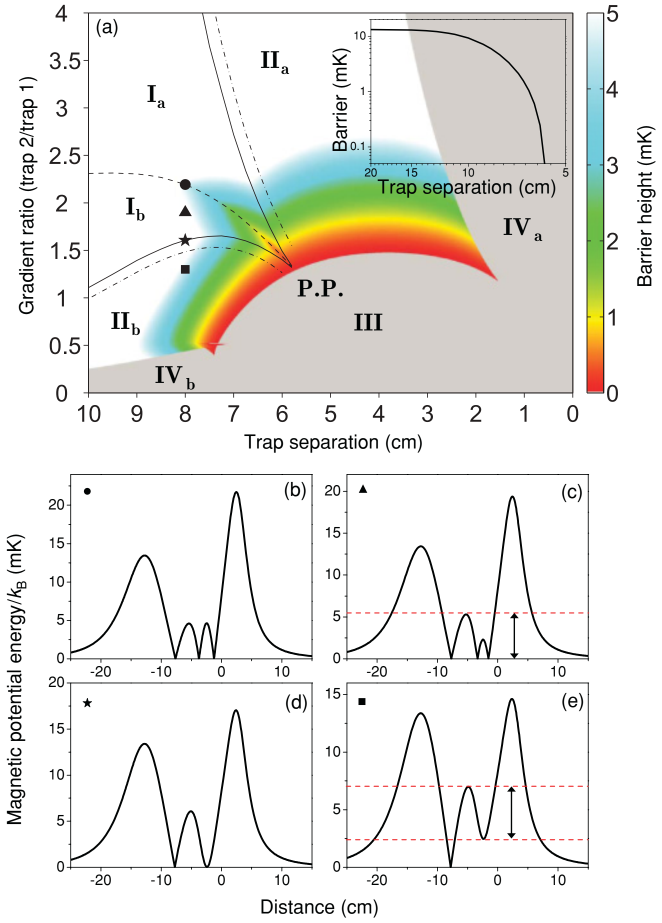

FIG. 2. (Color online) (a) Combined magnetic potential as a function of gradient ratio (trap 2:trap 1) and trap separation for ^{85}Rb ($F = 2, m_F = -2$), where the axial field gradient of trap 1 is 180 G cm^{-1}. The dashed black line indicates where the two inner potential barriers are maintained at an equal height and the inset of (a) shows how this barrier height changes as a function of the trap separation. The solid black lines show the trajectories where two zeros have merged and the resulting single minimum is about to lift up. The upper (lower) dash-dotted line represents where the trap 1 (trap 2) minimum is lifted to 1 mK. (b)–(e) show the combined potentials along the transport axis for the points marked in (a). Dashed red lines in (c) and (e) indicate the relevant barrier heights plotted in (a) as a color variation in mK for regions I and II, respectively. The pinch point referred to in the main text is labeled as PP.

how the combined magnetic potential changes with respect to gradient ratio for a fixed trap separation.

Understanding the potential map is fundamental to understanding the merging process, therefore, we will now discuss in detail the regions highlighted in Fig. 2(a). Regions with differing Roman numerals identify different qualitative behavior in the combined magnetic potential. In region I the combined magnetic potential exhibits three field zeros separated by two potential barriers [Figs. 2(b) and 2(c)]. Separating this region into two parts is the dashed line, along which the barriers are of equal height [Fig. 2(b)]. The barrier height along this line is shown, as a function of separation, in the inset of Fig. 2(a). On either side of the dashed line the barriers are asymmetric and smaller on the side of trap 1 (I_a) or trap 2 (I_B) [Fig. 2(c)]. In region II there are only two field minima and one barrier as the central field zero and either trap 1 (II_a) or trap 2 (II_B) have combined [Figs. 2(d) and 2(e)]. The solid black lines mark the boundary between regions I and II [Fig. 2(d)]. As we venture further into region II the magnetic field of the combined minimum becomes nonzero and increases in magnitude as we move further from the solid line [Fig. 2(e)]. The dash-dotted lines indicate where this minimum has been lifted to a potential of 1 mK. Note that all potential energies presented in this analysis refer to ^{85}Rb ($F = 2, m_F = -2$) and an axial field gradient of trap 1 equal to 180 G cm^{-1}.

The optimum merging strategy is to avoid the raised minima that occur in region II as the raised potential could heat the cloud. Consequently, the optimal merging channel is given by the boundaries of region I, where two intermediate barriers and three magnetic-field zeros continue to be maintained. The three lines guiding the channel converge and lead into region III at the pinch point [indicated in Fig. 2(a) by PP]. In region III (and region IV) traps 1 and 2 have merged into a single trap. As an aside, we note that the conveyorlike shifting of such single, merged traps operating permanently in region III has previously been demonstrated to great effect for the magnetic transport of ultracold atoms [43,46]; however, those experiments did not involve true merging in the sense employed in this work. In this simple picture we identify optimal trajectories as those that broadly follow the dashed line in region I passing through the merging channel and entering region III at the pinch point, thereby avoiding the raised minima in region II.

The color map in Fig. 2(a) represents the relevant barrier height and can be used to assess the extent of merging between the two atom clouds with finite energy. While the merging process is not adiabatic, to give some indication of the kinetic energy of atoms in the traps with respect to the inner barrier heights, we will treat the clouds as being in thermal equilibrium in the following analysis. We assume a temperature of 250 μK for a gas confined in a trap with an axial field gradient of 180 G cm^{-1}. In region I the color map indicates the maximum intermediate barrier height in mK, given by the dashed red line in Fig. 2(c). Within the white area of this region no merging occurs as less than 1% of atoms have sufficient kinetic energy to traverse potential barriers of height greater than 2.75 mK. Merging of the two traps begins to occur below a potential barrier height of approximately 2.75 mK; however, it is important to note that atoms from one trap may spill over the smaller barrier into the intermediate trap while the combined magnetic potential remains in region I. Once the trajectory reaches a barrier height of 1 mK, approximately 50% of atoms can traverse the inner barriers. In region II the color map shows the minimum relative barrier height, given by the dashed red lines in Fig. 2(e). Here atoms could suffer an undesirable gain in kinetic energy during merging as they may be dropped from the lifted nonzero minimum into the trap with a field zero. Introducing finite energy broadens the merging channel because individual traps can be lifted if the kinetic energy that results from dropping the atoms into the second trap is small in comparison with the initial thermal energy of the gas. The dash-dotted lines in Fig. 2(a) give an indication of this broadening for a tolerance of the trap lifting up to 1 mK.

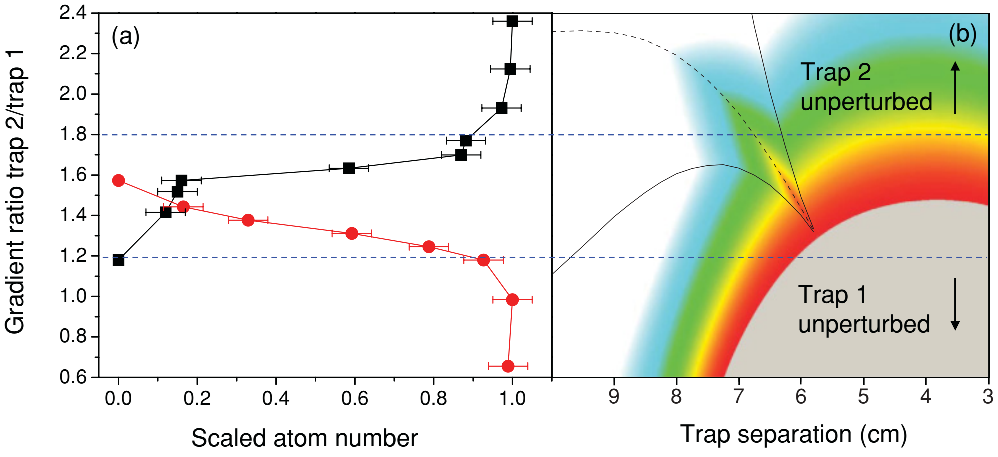

FIG. 3. (Color online) (a) Scaled atom number after merging as a function of the fixed gradient ratio of the two traps. The atoms are initially confined either in trap 2 (black squares) or in trap 1 (red circles). In both cases the second trap is initially empty. The dashed blue lines indicate the gradient ratios for each trap where 10% of the atoms are lost during a merge event. These lines are also shown in the potential map in (b) to highlight the regions where either trap 1 or trap 2 is largely unperturbed by the presence of the other trap.

In order to confirm the validity of the above analysis we identify two trajectories on Fig. 2(a) that we test experimentally in Sec. IV. The first of these trajectories is maintaining a constant gradient ratio during merging (see Fig. 3). We predict that for high or low gradient ratios atoms will only be maintained from the dominant trap and expect that poor merging will occur for intermediate ratios due to these not following the optimal trajectory. For our second trajectory we aim to maintain a gradient ratio that follows the dashed line in Fig. 2(a). Since merging only begins to occur below a barrier height of approximately 2.75 mK in region I, we choose a trajectory consisting of a constant gradient ratio followed by a ramp downward tangential to the dashed line below approximately 2.75 mK [see Fig. 5(a) inset]. We expect to observe optimal merging following such trajectories.

III. EXPERIMENTAL SETUP

In this section we present a brief description of the experimental setup. The apparatus is divided between two independent optical tables. The first table houses the laser system, which is used to prepare the necessary light frequencies for laser cooling, repumping, optical pumping, and imaging. The light is delivered by optical fibers to the second table on which the vacuum system, laser cooling, and magnetic trapping hardware is situated. A key feature of the apparatus is that, at any one time, the laser system only generates the light for either ^{85}Rb or ^{87}Rb, but the system can be easily switched from one isotope to the other during the course of an experimental run.

The laser setup consists of two commercial extended cavity diode lasers (Toptica DL100) and a tapered amplifier (Toptica BoosTA). Both the diode lasers operate on the 780-nm $5S_{1/2} \rightarrow 5P_{3/2}$ transition. The first laser generates the light for laser cooling and imaging and is stabilized to the cycling transition ($F = 3 \rightarrow F' = 4$ for ^{85}Rb or $F = 2 \rightarrow F' = 3$ for ^{87}Rb) using modulation transfer spectroscopy [47]. The necessary variable detunings required for laser cooling and absorption imaging are generated using several acousto-optical modulators (AOMs) in a double-pass configuration. The AOMs also allow real-time control of the light intensity. The tapered amplifier is used to increase the amount of light available for laser cooling. The second laser generates the light for repumping and optical pumping and is stabilized to the repump transition ($F = 2 \rightarrow F' = 3$ for ^{85}Rb or $F = 1 \rightarrow F' = 2$ for ^{87}Rb) using frequency-modulation spectroscopy [48]. Again AOMs are used for intensity control of the repump light. An additional AOM is used in a double- (single-) pass configuration to generate the optical pumping light for ^{85}Rb (^{87}Rb).

This versatile setup allows us to produce ultracold atomic gases of ^{85}Rb or ^{87}Rb by simply relocking the two extended cavity diode lasers to the equivalent transitions. This simple switch is only possible because the lasers are locked directly to the cycling and repump transitions. Alternative schemes, for example, stabilizing the laser frequency to a crossover resonance, require fewer AOMs but cannot be simply switched from one isotope to the other.

The vacuum system is divided into two sections connected by a differential pumping stage 6 mm in diameter and 28 mm in length including a 5-mm-diam aperture. Ultracold atoms are prepared in a standard six-beam MOT configuration [49] in a stainless-steel octagonal chamber. Here we typically load up to 10^9 ^{85}Rb atoms (or 7×10^8 ^{87}Rb atoms) in less than 10 s from a background vapor of rubidium supplied by a dispenser (SAES Getters). After a short compressed MOT phase and a molasses stage [50], we optically pump the atoms into the $F = 2, m_F = -2$ state for ^{85}Rb or the $F = 1, m_F = -1$ state for ^{87}Rb. The atoms are then loaded into a quadrupole trap (trap 1) with an axial field gradient of $50\,\mathrm{G\,cm^{-1}}$. The gradient is then adiabatically increased to $160\,\mathrm{G\,cm^{-1}}$ before the trap is transported over 50 cm along the vacuum system in 2.5 s to an UHV glass cell. The magnetic transport [43,44] is achieved by mounting the quadrupole trap on a motorized translation stage (Parker 404 series) thtat has a positioning accuracy of 5 μm. Movement of the translation stage can be programmed to follow a variety of velocity profiles, with accurate control of the speed and acceleration. Further details of the magnetic transport and the construction of the apparatus will be presented elsewhere.

Once in the UHV cell, the atoms are transferred to a second static quadrupole trap (trap 2). This is achieved by first fully overlapping the two sets of quadrupole coils and then adiabatically turning on the gradient of trap 2 to 320 G cm^{-1} while simultaneously decreasing the gradient of trap 1 to zero. The lifetime of the trapped gas in trap 2 is (240 ± 10) s and the observed heating rate is 0.30(2) μKs^{-1}. Having transferred the atoms to trap 2, trap 1 is returned to the MOT chamber to collect a second cloud of atoms, which is again transported to the UHV cell. The two trapped samples are then controllably merged by overlapping the two sets of coils, this time with currents flowing in both sets of coils. When the center of trap 1 is 10 cm away from the center of trap 2 the hardware controlling the motorized translation stage generates a trigger that is read by the main experimental control system. This allows subsequent ramps of the magnetic-field gradients to be precisely timed with respect to the motion of trap 1. Following such a merging sequence, the currents generating both traps are switched off in less than 0.2 ms and standard absorption imaging techniques are used to probe the temperature and density of the combined atomic cloud.

When merging experiments with two different isotopes are performed, we initially collect ^{85}Rb and then switch the laser frequencies as trap 1 returns to the MOT chamber in order to collect an equal number of ^{87}Rb atoms. To compensate partially for the difference of magnetic moment between ^{85}Rb ($m_F g_F = 2/3$) and ^{87}Rb ($m_F g_F = 1/2$), we increase the gradient of trap 1 while transporting ^{87}Rb to 205 G cm^{-1} (limited by heating in the coils).

IV. EXPERIMENTAL RESULTS

To test the predictions based upon the potential map in Fig. 2(a), we initially performed a series of merging experiments with ^{85}Rb atoms confined in both traps (Secs. IV A–IV C). Subsequently we demonstrate the merging of two different isotopes of rubidium (Sec. IV D).

A. Merging with fixed field gradients

Our initial aim was to investigate the first trajectory identified in Sec. II, that is, whether merging could be achieved for a fixed value of the gradient ratio. To test this we confined the atoms initially in either trap 1 or trap 2 and then merged the two traps with a velocity of 5 cm s^{-1} for a range of constant gradient ratios. In both cases the second trap was initially empty. The results of these simple experiments are shown in Fig. 3. Throughout the paper the measured atom number is scaled to the maximum number loaded into each trap before merging. For the results shown in Fig. 3, this corresponded to $(5.3 \pm 0.3) \times 10^8$ for trap 1 and $(7.0 \pm 0.4) \times 10^8$ for trap 2. The regions above and below the dashed blue lines identify the gradient ratios where less than 10% of the atoms are lost from either trap during the merging process and these lines are also indicated on the potential map. Henceforth, we shall refer to the dominant trap in each of these regions as being unperturbed. As predicted in Sec. II, at high gradient ratios trap 2 dominates trap 1. Evidence of this can be seen in Fig. 3(a), where atoms from the weaker trap 1 fail to enter the stronger trap 2. The converse can be seen for low gradient ratios. Also, as predicted, there is a smooth transition between the two unperturbed regions. However, the merging here is highly inefficient. For example, at a gradient ratio of approximately 1.5, where the atom number is equal for both traps, only approximately 15% of the atoms are retained from each of the traps.

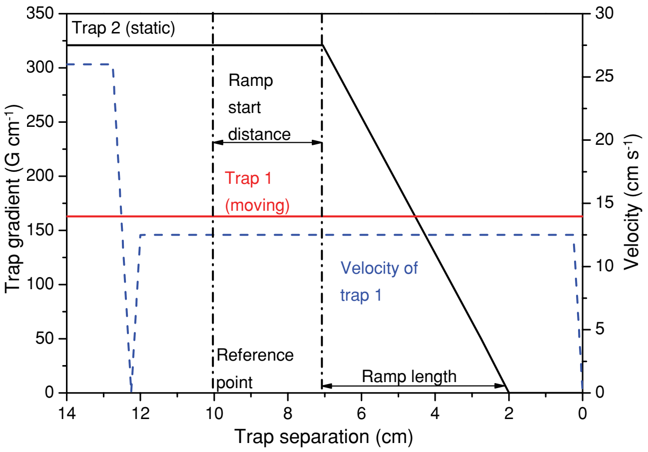

FIG. 4. (Color online) Typical evolution profiles of the gradient and velocity of the quadrupole traps during merging. The gradient of trap 1 (lower solid red line) remains constant, while the gradient of trap 2 (upper solid black line) is decreased during the merging process. The dashed blue line shows the velocity profile of trap 1, which decreases from the transport setting to a new variable velocity before the merging begins.

B. Merging with ramped field gradients

In order to discover whether successful merging could be achieved by following the narrow merging channel of region I, we employed a linear ramp of the gradient ratio during the merging as depicted in Fig. 4. In this scenario the gradient in trap 1 is held constant at 160 G cm^{-1} as it is moved toward the static trap 2. At a separation of 10 cm, where the traps are far from the merging region [see Fig. 2(a)], the reference trigger from the hardware controlling the motorized translation stage is sent to our control system. After trap 1 has traveled a variable distance beyond this reference point, which we refer to as the ramp start distance, the gradient of trap 2 is linearly decreased from the initial 320 G cm^{-1} to zero over a variable time. In order for the data to be comparable to Fig. 2(a) we relate the time taken for this linear ramp to the distance that the trap separation has decreased in this time and define it as the ramp length. The velocity of trap 1 is altered from the transport setting (26 cm s^{-1}) to a new variable velocity before the merging begins, as depicted in Fig. 4. By varying the ramp start distance and the ramp length we are able to explore the potential map in Fig. 2(a), searching for the optimum merging trajectory.

In a first set of experiments, we fixed the ramp length and varied the ramp start distance, thus translating the ramp horizontally [with respect to Figs. 2(a) and 4] across the merging channel and the pinch point. For each experiment the merging was performed three times: first with the atoms in trap 1, then with the atoms in trap 2, and finally with the atoms loaded into both traps. The results in Fig. 5(a) are for a ramp length of 3 cm, merging speed of 12.5 cm s^{-1}, and initial atom number of 1.5×10^8. The left-hand side of this figure corresponds to an experiment where effectively trap 2 is turned off before trap 1 arrives and, accordingly, all the atoms initially in trap 1 remain. The right-hand side of the figure corresponds to an experiment where trap 1 and trap 2 are effectively merged with a constant gradient ratio (equal to 2 in this case). In this limit, therefore, the results are consistent with the experiment presented in Fig. 3, with the majority of the atoms initially in trap 2 remaining. In the central region of the figure a mixture of atoms from trap 1 and trap 2 remain in the merged trap. The solid blue line in the inset of Fig. 5(a) depicts the ramp given by the circled data point, which clearly follows the identified merging channel, passing very close to the pinch point. In this case, highly improved merging is observed for an optimum ramp start distance of 6.7 ± 0.1 cm when compared to the fixed gradient case shown in Fig. 3.

We then repeated this experiment for several ramp lengths, with the aim of confirming the existence of the pinch point. In each case we were able to identify an optimum ramp start distance for the given ramp length by requiring that approximately equal numbers of atoms were transferred from each trap into the final merged trap. Strikingly, within experimental error, the optimum ramps intersect and we identify an experimental pinch point of (trap separation, gradient ratio) = (5.8 ± 0.1cm, 1.4 ± 0.1). This is in remarkably good agreement with the theoretically determined pinch point of (5.76 cm, 1.30). Moreover, closer examination of these data highlights that the most successful merging occurs for trajectories that follow the merging channel. These results therefore confirm our predictions that the optimum merging trajectory will follow the merging channel and will pass through the narrow pinch point.

C. Optimizing the merging trajectory

To test the dependence of the merging on the slope of the trajectory, we performed a second set of experiments in which the ramp length was varied while the ramp start distance was adjusted to ensure that the trajectory still passed through the experimentally determined pinch point, effectively swiveling around this point [see the double-headed arrow in Fig. 5(b) inset]. Traps 1 and 2 were again loaded with equal numbers of atoms and the combined atom number after merging was measured. The results are plotted in Fig. 5(b), identifying an optimum ramp length of (4.0 ± 0.5) cm through the experimentally determined pinch point. This merging trajectory through the potential map is entirely consistent with our theoretical predictions in Sec. II and there is excellent agreement between the slope of the trajectory and the gradient of the dashed line in Fig. 2(a) in the vicinity of the pinch point [see the solid blue line in the inset of Fig. 5(b)]. Note, however, that the uncertainty in the optimum ramp length, due to the broad peak seen in Fig. 5(b), is an indication of the presence of a broadened merging channel.

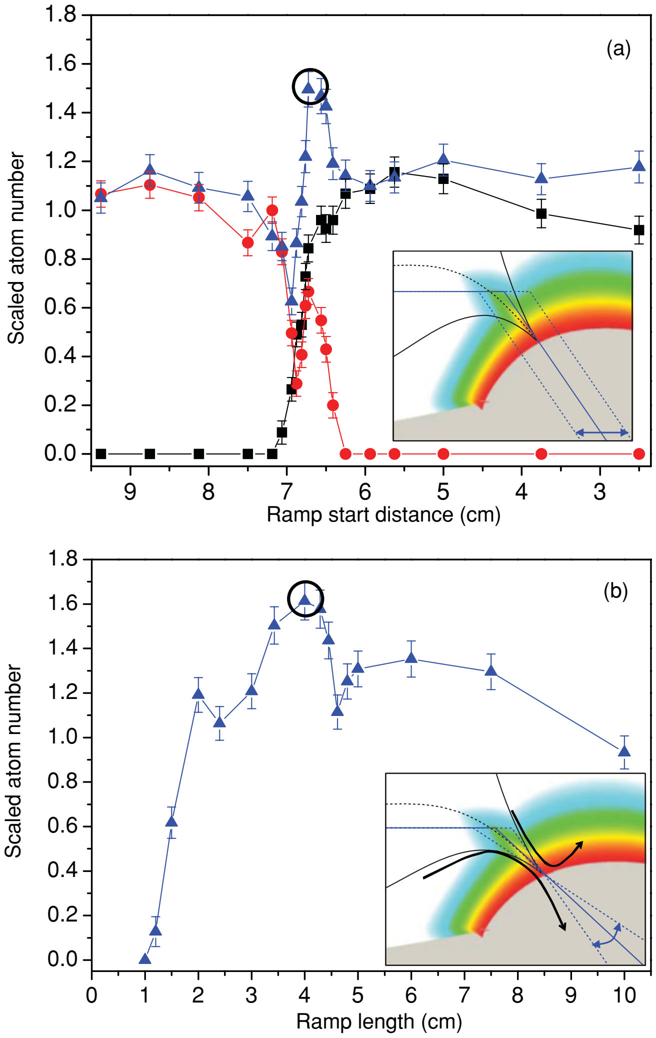

FIG. 5. (Color online) Optimizing the merging process through measurements of the scaled atom number following the merging as a function of the ramp parameters. In (a) we vary the ramp start position, for a ramp length of 3.0 cm, translating the ramp across the pinch point and in (b) we vary the ramp length, i.e., the angle of the trajectory through the pinch point. Data are shown for atoms initially in trap 2 (black squares), trap 1 (red circles), and both traps (blue triangles). The solid blue lines in the insets indicate the ramps circled in each figure, while the dotted blue lines indicate the variation of the ramp in each experiment. The results of a large number of experimentally tested ramps are summarized in the inset of (b) with the single-headed curved black arrows indicating where the merged atom number is approximately 50% of that seen for the optimal trajectory.

Having established the optimum merging trajectory for the experimentally determined pinch point, we carried out many more runs varying the trajectory around this optimum in order to estimate the size and width of the merging channel. The results are summarized in the inset of Fig. 5(b). The black single-headed curved arrows indicate trajectories where the merged atom number is half of the number obtained along the optimum trajectory. As theoretically predicted in Sec. II, the channel narrows into the crucial pinch point and then opens wide once merging is achieved, with the black single-headed arrows confirming the broadening of the pinch point due to the finite temperature of the atoms.

In a further experiment, we also varied the velocity of trap 1 during the merging for this optimum ramp length. This showed that, within the experimental uncertainties, the maximum achievable atom number is independent of the speed with which the two traps merge up to 12.5 cm s^{-1}. For higher speeds the number of atoms remaining in trap 1 falls off quickly toward zero.

Using the optimum ramp length determined from Fig. 5(b), we made a detailed measurement of the atom number and the temperature for the merged cloud as a function of the ramp start distance for ^{85}Rb in both traps (see Fig. 6). The results indicate that a merge of approximately 75% of the atoms from each trap was possible giving approximately 150% of the number achieved in a single load. In addition, we do not observe any significant heating with the final merged clouds having typical temperatures of approximately 300 μK to be compared with the temperatures of the initial clouds of approximately 260 μK.

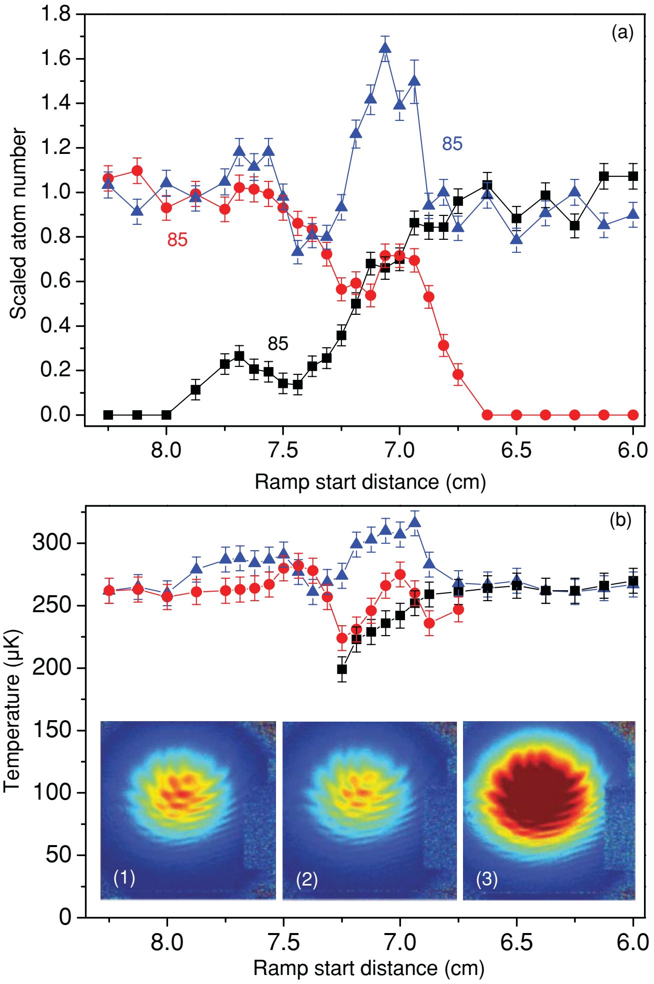

FIG. 6. (Color online) Detailed results of the merging for ^{85}Rb. Shown are (a) the scaled atom number and (b) temperature following the merging [for atoms initially in trap 2 (black squares), trap 1 (red circles), and both traps (blue triangles)] as a function of the ramp start distance for a fixed ramp length of 4.0 cm, initial gradient ratio of 2, and a merging speed of 12.5 cm s^{-1}. The inset in (b) shows false color absorption images of the atomic cloud following merging [for atoms initially in (1) trap 1, (2) trap 2, and (3) both traps]. Both traps contained a maximum number of 3.5×10^8 atoms.

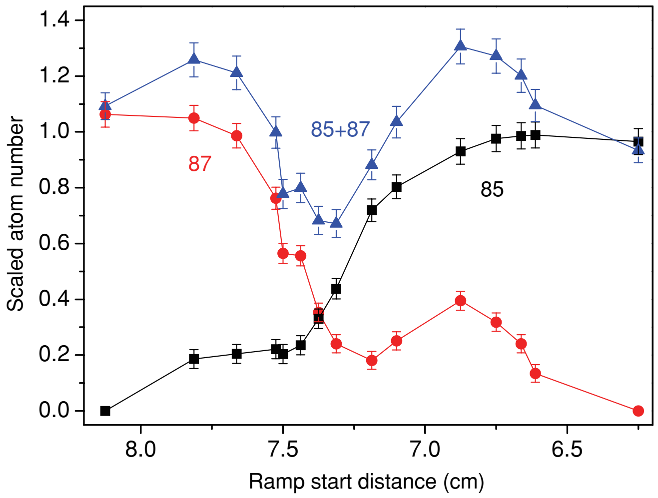

FIG. 7. (Color online) Merging of the two rubidium isotopes using the optimum ramp length and merging speed determined in the ^{85}Rb experiments. Scaled atom number is shown as a function of the ramp start distance. ^{85}Rb is held initially in trap 2 and then merged with ^{87}Rb in trap 1.

D. Merging ^{85}Rb and ^{87}Rb

In a final experiment, we demonstrated the merging of the two different rubidium isotopes as shown in Fig. 7 by simply using the optimum ramp length determined for ^{85}Rb. Throughout this experiment, we ensured that the number of ^{87}Rb atoms in trap 1 prior to the merging was the same as the number of ^{85}Rb present in trap 2. In this case we were only able to achieve an equal merge of approximately 40% from each isotope, primarily due to poorer transfer of ^{87}Rb into the combined trap. We believe this is due to a technical limitation whereby we were unable to completely compensate for the smaller magnetic moment of ^{87}Rb ($\mu_{87} = \frac{3}{4}\mu_{85}$). To regain the same trap stiffness as for ^{85}Rb the magnetic-field gradient has to increase by $\frac{4}{3}$; however, this was not possible due to the current limit of the power supply to the coils. We note that for sympathetic cooling it is desirable to start with a high ratio of refrigerant species to the species to be cooled, e.g., greater than 30:1 (^{87}Rb:^{85}Rb) [30,36]. Hence, despite this poorer merging efficiency, we are able to create suitable conditions for sympathetic cooling of ^{85}Rb with ^{87}Rb, either by choosing the appropriate ramp start distance or by simply loading less ^{85}Rb into trap 2. Specifically, we have loaded 1.5×10^8 ^{87}Rb atoms with 5×10^7 ^{85}Rb atoms at a temperature of approximately 200 μK, enabling straightforward access to similar starting conditions to experiments that employ separate laser-cooling setups for each isotope [30,36].

V. DISCUSSION AND CONCLUSION

Before concluding we mention two more points of interest regarding our experimental results. First, all the experiments described have been repeated at least twice over several months and the detailed structure seen in the merging plots of Fig. 5(a), 6(a), and 7 is reproducible. We believe this is related to the dynamics of the atoms as they cross the magnetic potential barriers outlined in our analysis in Sec. II. This demonstrates the need for precise control and synchronization of the transport mechanism with the gradient ramps in order to achieve reproducible merging. Second, despite our best effort to obtain merging of approximately 100% of the atoms from each trap, we were only able to achieve approximately 75% of each ^{85}Rb cloud. A possible explanation is that more energetic atoms in the cloud are colliding with the surface of our vacuum chamber. However, we have repeated the merging with initial cloud temperatures of approximately 260 and approximately 70 μK and saw no improvement in the merging percentage for the colder atoms. An alternative explanation is that we experience enhanced Majorana losses as the intermediate trap barriers are reduced to zero during the merging. The extent of the region of magnetic field where Majorana losses will occur again depends sensitively on the exact trajectory through the potential map and this fact may also contribute to the detailed structure seen in the merging plots.

In general, the technique of magnetic merging we have described allows the merging of any two magnetically trappable species and is not limited to the case of an isotopic mixture. It offers an advantage whenever two atom clouds cannot be laser cooled in the same trap; for instance, it circumvents the problem of detrimental light-assisted collisions that occur in some two-species magneto-optical traps [33,34]. Such collisions often severely limit the achievable range of atom numbers (and their ratios) in the MOT. We believe that as experiments in the field become ever more complex and sophisticated, techniques such as the magnetic merging will become essential to access new physics in these rich systems. The merging process can in principle be repeated several times allowing the generation of even more complex mixtures comprising three [4] or more species. This could greatly extend the range of possible physics in mixture experiments. Also our analysis of the merging process is extendable to other trap geometries and may therefore be of interest to the atom chip community.

Modern Bose-Einstein condensate experiments with differentially pumped vacuum chambers tend to fall into two camps, those employing a push beam with a double MOT system or Zeeman slower to collect atoms separately from the ultrahigh-vacuum science chamber or those employing a magnetic transport system to achieve the same separation of collection and science zones. The latter method offers the advantages of very long lifetimes in the science cell combined with excellent optical access owing to the lack of MOT optics. Certainly in these magnetic transport systems it is a relatively simple matter to implement the magnetic merging that we have described as it is primarily a matter of synchronizing the magnetic-field-generating currents with the pre-existing coil motion.

In our specific case of ^{85}Rb and ^{87}Rb we were able to use just one laser-cooling system (i.e., a cooling laser and a repumping laser with associated AOMs, optics, and fibers) to load each isotope at separate times before magnetic merging. This considerable simplification allowed stable and reproducible loading of the number of atoms of each isotope over a large range from zero to 5×10^8 for each species and the ratio of the atomic numbers can be further tailored reproducibly during the merging process. Specifically, the technique allows equal ratio mixtures to be realized, which is often difficult in two-species MOTs.

In conclusion, we have demonstrated the magnetic merging of two ultracold atomic gases by the controlled overlap of two initially well-separated magnetic quadrupole traps. We have shown that a simple one-dimensional analysis of the combined magnetic-field potential as the two traps are brought together is sufficient to identify and understand the region where merging occurs and leads to a clear prediction of the optimum trajectory for the merging. We have verified this prediction experimentally using ^{85}Rb and found that the final atom number in the merged trap is maximized with minimal heating by following the predicted optimum trajectory. We believe that optimal merging trajectories could be determined for any specific coil geometries and sizes by following a similar methodology. We have used the merging technique to multiply load atoms into a single magnetic quadrupole trap. While this did not produce an increase in phase-space density, the accumulation of atoms in a single trap can be beneficial for subsequent evaporative cooling. Finally, we have used the magnetic merging to create controlled variable-ratio atomic mixtures of the two isotopes of rubidium into a single quadrupole trap with a simple laser system for laser cooling each isotope sequentially.

ACKNOWLEDGMENTS

We acknowledge support from the UK Engineering and Physical Sciences Research Council (Grants No. EP/F002068/1 and No. EP/G026602/1) and the European Science Foundation within the EUROCORES Programme EuroQUASAR. S.L.C acknowledges the support of the Royal Society.

APPENDIX

Table I summarizes the parameters of the coils used in the experiment to generate the two quadrupole traps.

TABLE I. Parameters of the physical and equivalent coils used to generate quadrupole traps 1 and 2. All the coils are wound from square cross-section copper tubing. The axial field gradient and the field maximum apply to the pair of coils in each case.

Parameter	Trap 1	Trap 2
Number of turns N	3 × 8	3 × 3
Tubing dimensions (mm × mm)	4.0 × 4.0	3.5 × 3.5
Inner separation (cm)	8.6(1)	3.7(1)
Outer separation (cm)	11.1(1)	5.9(1)
Inner radius (cm)	3.0(1)	2.2(1)
Outer radius (cm)	6.5(1)	3.4(1)
Equivalent coil separation (cm)	10.4(1)	4.7(1)
Equivalent coil radius (cm)	4.9(1)	2.7(1)
Axial field gradient (G cm^{-1}A^{-1})	0.606(1)	0.974(1)
Field maximum (GA $^{-1}$)	1.004	0.961

[1] C. J. Myatt, E. A. Burt, R. W. Ghrist, E. A. Cornell, and C. E. Wieman, Phys. Rev. Lett. **78**, 586 (1997).

[2] J. Stenger, S. Inouye, D. M. Stamper-Kurn, H.-J. Miesner, A. P. Chikkatur, and W. Ketterle, Nature **396**, 345 (1998).

[3] A. G. Truscott, K. E. Strecker, W. I. McAlexander, G. B. Partridge, and R. G. Hulet, Science **291**, 2570 (2001).

[4] Z. Hadzibabic, C. A. Stan, K. Dieckmann, S. Gupta, M. W. Zwierlein, A. Görlitz, and W. Ketterle, Phys. Rev. Lett. **88**, 160401 (2002).

[5] G. Roati, F. Riboli, G. Modugno, and M. Inguscio, Phys. Rev. Lett. **89**, 150403 (2002).

[6] G. Modugno, M. Modugno, F. Riboli, G. Roati, and M. Inguscio, Phys. Rev. Lett. **89**, 190404 (2002).

[7] C. Silber, S. Günther, C. Marzok, B. Deh, P. W. Courteille, and C. Zimmermann, Phys. Rev. Lett. **95**, 170408 (2005).

[8] M. Zaccanti, C. D'Errico, F. Ferlaino, G. Roati, M. Inguscio, and G. Modugno, Phys. Rev. A **74**, 041605 (2006).

[9] S. Ospelkaus, C. Ospelkaus, O. Wille, M. Succo, P. Ernst, K. Sengstock, and K. Bongs, Phys. Rev. Lett. **96**, 180403 (2006).

[10] S. B. Papp, J. M. Pino, and C. E. Wieman, Phys. Rev. Lett. **101**, 040402 (2008).

[11] M. Taglieber, A.-C. Voigt, T. Aoki, T. W. Hänsch, and K. Dieckmann, Phys. Rev. Lett. **100**, 010401 (2008).

[12] M. K. Tey, S. Stellmer, R. Grimm, and F. Schreck, Phys. Rev. A **82**, 011608 (2010).

[13] M. Trippenbach, K. Góral, K. Rzazewski, B. Malomed, and Y. B. Band, J. Phys. B **33**, 4017 (2000).

[14] E. Altman, W. Hofstetter, E. Demler, and M. D. Lukin, New J. Phys. **5**, 113 (2003).

[15] A. Kuklov, N. Prokof'ev, and B. Svistunov, Phys. Rev. Lett. **92**, 050402 (2004).

[16] A. Micheli, G. K. Brennen, and P. Zoller, Nature Phys. **2**, 341 (2006).

[17] D. DeMille, Phys. Rev. Lett. **88**, 067901 (2002).

[18] S. Giorgini, L. P. Pitaevskii, and S. Stringari, Rev. Mod. Phys. **80**, 1215 (2008).

[19] L. D. Carr, D. DeMille, R. V. Krems, and J. Ye, New J. Phys. **11**, 055049 (2009).

[20] T. Köhler, K. Góral, and P. S. Julienne, Rev. Mod. Phys. **78**, 1311 (2006).

[21] C. Chin, R. Grimm, P. Julienne, and E. Tiesinga, Rev. Mod. Phys. **82**, 1225 (2010).

[22] K. M. Jones, E. Tiesinga, P. D. Lett, and P. S. Julienne, Rev. Mod. Phys. **78**, 483 (2006).

[23] J. M. Sage, S. Sainis, T. Bergeman, and D. DeMille, Phys. Rev. Lett. **94**, 203001 (2005).

[24] J. G. Danzl, E. Haller, M. Gustavsson, M. J. Mark, R. Hart, N. Bouloufa, O. Dulieu, H. Ritsch, and H. Nägerl, Science **321**, 1062 (2008).

[25] F. Lang, K. Winkler, C. Strauss, R. Grimm, and J. Hecker Denschlag, Phys. Rev. Lett. **101**, 133005 (2008).

[26] K.-K. Ni, S. Ospelkaus, M. H. G. de Miranda, A. Pe'er, B. Neyenhuis, J. J. Zirbel, S. Kotochigova, P. S. Julienne, D. S. Jin, and J. Ye, Science **322**, 231 (2008).

[27] M. Viteau, A. Chotia, M. Allegrini, N. Bouloufa, O. Dulieu, D. Comparat, and P. Pillet, Science **321**, 232 (2008).

[28] J. Deiglmayr, A. Grochola, M. Repp, K. Mörtlbauer, C. Glück, J. Lange, O. Dulieu, R. Wester, and M. Weidemüller, Phys. Rev. Lett. **101**, 133004 (2008).

[29] T. Lahaye, C. Menotti, L. Santos, M. Lewenstein, and T. Pfau, Rep. Prog. Phys. **72**, 126401 (2009).

[30] P. A. Altin, N. P. Robins, D. Döring, J. E. Debs, R. Poldy, C. Figl, and J. D. Close, Rev. Sci. Instrum. **81**, 063103 (2010).

[31] G. Thalhammer, G. Barontini, L. De Sarlo, J. Catani, F. Minardi, and M. Inguscio, Phys. Rev. Lett. **100**, 210402 (2008).

[32] W. Ketterle and M. W. Zwierlein, Rivista del Nuovo Cimento **31**, 247 (2008).

[33] J. Weiner, V. S. Bagnato, S. Zilio, and P. S. Julienne, Rev. Mod. Phys. **71**, 1 (1999).

[34] M. L. Harris, P. Tierney, and S. L. Cornish, J. Phys. B **41**, 035303 (2008).

[35] J. P. Burke Jr., J. L. Bohn, B. D. Esry, and C. H. Greene, Phys. Rev. Lett. **80**, 2097 (1998).

[36] S. B. Papp and C. E. Wieman, Phys. Rev. Lett. **97**, 180404 (2006).

[37] I. Bloch, M. Greiner, O. Mandel, T. W. Hänsch, and T. Esslinger, Phys. Rev. A **64**, 021402 (2001).

[38] S. L. Cornish, N. R. Claussen, J. L. Roberts, E. A. Cornell, and C. E. Wieman, Phys. Rev. Lett. **85**, 1795 (2000).

[39] J. L. Roberts, N. R. Claussen, S. L. Cornish, E. A. Donley, E. A. Cornell, and C. E. Wieman, Phys. Rev. Lett. **86**, 4211 (2001).

[40] E. A. Donley, N. R. Claussen, S. L. Cornish, J. L. Roberts, E. A. Cornell, and C. E. Wieman, Nature (London) **412**, 295 (2001).

[41] S. L. Cornish, S. T. Thompson, and C. E. Wieman, Phys. Rev. Lett. **96**, 170401 (2006).

[42] J. F. Bertelsen, H. K. Andersen, S. Mai, and M. Budde, Phys. Rev. A **75**, 013404 (2007).

[43] M. Greiner, I. Bloch, T. W. Hänsch, and T. Esslinger, Phys. Rev. A **63**, 031401 (2001).

[44] H. J. Lewandowski, D. M. Harber, D. L. Whitaker, and E. A. Cornell, J. Low Temp. Phys. **132**, 309 (2003).

[45] A. L. Migdall, J. V. Prodan, W. D. Phillips, T. H. Bergeman, and H. J. Metcalf, Phys. Rev. Lett. **54**, 2596 (1985).

[46] W. Hänsel, J. Reichel, P. Hommelhoff, and T. W. Hänsch, Phys. Rev. Lett. **86**, 608 (2001).

[47] D. J. McCarron, S. A. King, and S. L. Cornish, Meas. Sci. Technol. **19**, 105601 (2008).

[48] G. C. Bjorklund, Opt. Lett. **5**, 15 (1980).

[49] E. L. Raab, M. Prentiss, A. Cable, S. Chu, and D. E. Pritchard, Phys. Rev. Lett. **59**, 2631 (1987).

[50] S. Chu, L. Hollberg, J. E. Bjorkholm, A. Cable, and A. Ashkin, Phys. Rev. Lett. **55**, 48 (1985).